Mitochondrial Phosphoenolpyruvate Carboxykinase Regulates Osteogenic Differentiation by Modulating AMPK/ULK1-Dependent Autophagy

ZHENG LI [ID],[a,b] XUENAN LIU,[a,b] YUAN ZHU,[a,b] YANGGE DU,[a,b] XUEJIAO LIU,[a,b] LONGWEI LV,[a,b] XIAO ZHANG,[a,b] YUNSONG LIU,[a,b] PING ZHANG,[a,b] YONGSHENG ZHOU[a,b]

Key Words. Autophagy • Mesenchymal stem cells • Osteogenic differentiation • Mitochondrial phosphoenolpyruvate carboxykinase

[a]Department of Prosthodontics, School and Hospital of Stomatology, Peking University, Beijing, People's Republic of China; [b]National Engineering Lab for Digital and Material Technology of Stomatology, National Clinical Research Center for Oral Diseases, Peking University School and Hospital of Stomatology, Peking University, Beijing, People's Republic of China

Correspondence: Ping Zhang, Ph.D., Department of Prosthodontics, Peking University School and Hospital of Stomatology, 22 Zhongguancun South Avenue, Haidian District, Beijing 100081, People's Republic of China. Telephone: 86-10-82195370; e-mail: zhangping332@bjmu.edu.cn; or Yongsheng Zhou, D.D.S., Ph.D., Vice Dean of the School, Chair and Professor of Department of Prosthodontics, Peking University School and Hospital of Stomatology, 22 Zhongguancun South Avenue, Haidian District, Beijing 100081, People's Republic of China. Telephone: 86-10-82195370; e-mail: kqzhouysh@hsc.pku.edu.cn

ABSTRACT

Mitochondrial phosphoenolpyruvate carboxykinase (PCK2) is a rate-limiting enzyme that plays critical roles in multiple physiological processes. The decompensation of PCK2 leads to various energy metabolic disorders. However, little is known regarding the effects of PCK2 on osteogenesis by human mesenchymal stem cells (hMSCs). Here, we report a novel function of PCK2 as a positive regulator of MSCs osteogenic differentiation. In addition to its well-known role in anabolism, we demonstrate that PCK2 regulates autophagy. PCK2 deficiency significantly suppressed autophagy, leading to the impairment of osteogenic capacity of MSCs. On the other hand, autophagy was promoted by PCK2 overexpression; this was accompanied by increased osteogenic differentiation of MSCs. Moreover, PCK2 regulated osteogenic differentiation of MSCs via AMP-activated protein kinase (AMPK)/unc-51 like autophagy activating kinase 1(ULK1)-dependent autophagy. Collectively, our present study unveiled a novel role for PCK2 in integrating autophagy and bone formation, providing a potential target for stem cell-based bone tissue engineering that may lead to improved therapies for metabolic bone diseases. STEM CELLS 2019;37:1542–1555

SIGNIFICANCE STATEMENT

The degradation substances from autophagy can be used as optional nutrient supply for cell survival and differentiation, making autophagy a suitable energy-refueling process during osteogenesis by mesenchymal stem cells (MSCs). Although mitochondrial phosphoenolpyruvate carboxykinase (PCK2) has been suggested as a critical enzyme for anabolism, it has been unclear whether PCK2 plays critical roles in autophagy. The study first determines that PCK2 promotes osteogenic differentiation by positively regulating autophagy in MSCs, which facilities better application of bone tissue engineering and maintenance of bone homeostasis.

INTRODUCTION

Due to the ease of their accessibility and their multipotent properties, mesenchymal stem cells (MSCs) have emerged as promising candidates for use in bone tissue engineering to repair bone defects [1]. Exploration of mechanisms underlying differentiation of MSCs toward osteogenic lineages may facilitate improved clinical application of MSCs in the treatment of metabolic bone diseases, which confers significant burden for patients and the healthcare system.

During the process of forming new bone matrix and mineral deposition, MSCs can encounter deficiencies in energy supply, and may have difficulty meeting the increased metabolic demand associated with self-renewal and osteogenic differentiation [2]. Under these conditions, anabolism in MSCs is elevated to ensure a sufficient energy supply, including reduced glycolysis and increased mitochondrial respiration [3]. With the increase of anabolism, useless organelles and metabolites accumulate in cells. To maintain homeostasis in MSCs, the amount of cellular proteins and organelles should be strictly restricted. Autophagy is a degradative mechanism by which cells remove damaged and dysfunctional components to recycle macromolecules and provide energy under the stress of differentiation [4]. Amino acids from organelles degraded by autophagy can be used as an optional nutrient supply for cell survival [5], making autophagy a suitable energy-refueling process during osteogenesis by MSCs. Previous studies have found the levels of autophagosomes present in MSCs [6, 7] is higher than that of many

differentiated cells. The autophagic flux was observed in early MSC osteogenesis, suggesting that autophagy is critical in MSC differentiation [7]. Activation of autophagy was reported to significantly increase osteogenic differentiation and could rescue bone volume (BV) [8]. Impaired autophagy was also found in the well-known skeletal degenerative diseases—osteoporosis [9]. These studies suggest that autophagy, as a vital link in the chain of energy metabolism, has a profound impact on the osteogenesis by MSCs. However, the regular mechanisms between autophagy and osteogenesis by MSCs have not been elaborately demonstrated.

Under conditions of nutrient-deprivation environment, gluconeogenesis is the primary source for endogenous glucose production [10]. Phosphoenolpyruvate carboxykinase (PEPCK) is an important enzyme in gluconeogenesis that catalyzes the decarboxylation of oxaloacetate (OAA) to phosphoenolpyruvate (PEP) in the tricarboxylic acid (TCA) cycle. Subsequently, through the activity of various enzymes in the glycolytic pathway, PEP can be transformed to glucose [11]. There are two isoforms of PEPCK: a cytosolic isoform (PEPCK1 or phosphoenolpyruvate carboxykinase [PCK1]) and a mitochondrial isoform (PEPCK2 or PCK2). Although the physiological function and regulatory patterns of PCK1 have been extensively explored [12, 13], the biological role of PCK2 is poorly understood. It has been reported that the stability of PCK1 [14] is regulated by acylation, and that hyperacetylated PCK1 can promote anaplerotic activity [15]. Additionally, PCK1 promotes the ability of cells to uptake glucose and glutamine by increasing the metabolism of fatty acids and nucleic acids [12]. Nevertheless, a mitochondrial mtGTP/PCK2 signaling may regulate glucose homeostasis by modulating the production and clearance of glucose, which suggests a role for PCK2 as a "metabolic tachometer" to sense TCA cycle flux [16]. Under low-glucose conditions, PCK2 allows cells to produce PEP from glutamine, which is used as a biosynthetic intermediate [17]. Therefore, the essential function of PCK2 in regulating gluconeogenesis is required for cells in a nutrient-deficient environment [18]. In light of the increasing energy demands during osteogenic differentiation, we wondered if PCK2 modulates osteogenic differentiation by influencing the cellular metabolic network.

The decompensation of PCK2 could lead to a series of energy metabolic disorders, such as diabetes mellitus [19] and glucose intolerance [20], which will further lead to bone metabolic diseases. Exploration of the role of PCK2 in regulating osteogenesis is central to the understanding of the pathogenesis and treatment of skeletal diseases such as osteoporosis. In the current study, we discovered that PCK2 is a positive regulator of osteogenesis by MSCs and serves an indispensable role in autophagy. Mechanistically, PCK2 promotes the osteogenic capacity of MSCs through AMP-activated protein kinase (AMPK)/unc-51 like autophagy activating kinase 1 (ULK1)-mediated autophagy. This study was the first to emphasize the vital role of PCK2 in promoting the osteogenic capacity of MSCs by regulating autophagy, which may lead to the establishment of new strategies for bone tissue engineering. Moreover, therapeutic intervention by targeting PCK2 in certain types of metabolic disorders might be beneficial.

MATERIALS AND METHODS

Cell Culture

The human adipose-derived stem cells (hASCs) and human bone marrow mesenchymal stem cells (hBMSCs) used in our study were obtained from ScienCell Research Laboratory (Carlsbad, CA). Cells in this study were between three and five passages and obtained from three healthy adult donors. All materials used in cell culture were bought from Sigma–Aldrich (St. Louis, MO). For the in vitro experiments, proliferation medium (PM) for hASCs consisted of fetal bovine serum (FBS; 10%, vol/vol), penicillin G (100 U/ml), and streptomycin (100 mg ml) into Dulbecco's modified Eagle's medium; the PM for hBMSCs consisted of Minimum Essential Medium α (α-MEM, Gibco, Grand island, USA), 10% (vol/vol) FBS, penicillin G (100 U/ml), and streptomycin (100 mg/ml). Dexamethasone (100 nM), L-ascorbic acid (200 mM), and β-glycerophosphate (10 mM) were added into PM to make osteogenic medium (OM). The cell culture conditions were 95% air, 5% CO_2, 100% relative humidity, and 37°C.

Lentiviral Transfection

Lentiviral transfection was performed as previously described [21]. Lentiviruses targeting PCK2 (sh1-*PCK2*, sh2-*PCK2*) and negative control (NC) vectors (NC1/NC2) were purchased from GenePharma Co. (Suzhou, China). Lentiviruses targeting ATG7 (sh1-*ATG7*, sh2-*ATG7*), NC, and lentiviruses containing PCK2 and the scramble control (vector) were purchased from Vector Builder Co. (Guangzhou, China). Multiplicity of infection of 100 was found to be suitable for transfection. When cells were exposed to the viral suspension, 5 mg/ml polybrene (Sigma) was added. After 72–96 hours, cells were incubated with puromycin (1 μg/ml, Sigma–Aldrich). The shRNA sequences used for PCK2 and ATG7 knockdown are shown in Table 1.

RNA Interference and Plasmid Transfection

The sequences of short interfering (si) RNAs targeting ULK1 (si1-*ULK1*, si2-*ULK1*) and the negative control (si-NC) are listed in Table 1 and were purchased from GenePharma Co. The si-RNA targeting AMP-activated protein kinase (si-AMPK) was obtained from HanBio (Shanghai, China). The pCIP-AMPKα1_WT plasmid was a gift from Reuben Shaw (Addgene plasmid # 79010; http://n2t.net/addgene:79010; RRID: Addgene_79010). The wild-type PCK2 (pEnCMV-PCK2-3 × FLAG) and mutant PCK2 plasmids (pEnCMV-PCK2-K261.262R-3 × FLAG) were constructed. Based on the manufacturer instructions, Lipofectamine 3000 (Invitrogen, Carlsbad, USA) was used as a transfection agent. After 48 hours, cells were collected and gene expressions were analyzed. During the process of osteogenesis, transfection was repeated every 5 days to ensure transfection efficiency and hASCs were harvested at 7 and 14 days after osteogenic induction.

Cell Proliferation Assay

Cells were seeded in 96-well plates at a density of ∼2×10^3 cells per well. At days 1–8, cells were incubated with 20 μl cell counting kit-8 (CCK-8) assay kit to analyze cell proliferation (Dojindo Laboratories, Kumamoto, Japan). After 1.5 hours at 37°C, the absorbance at 490 nm was measured for each well, and cell proliferation curves were plotted. The experiments were repeated at least three times. Each group was tested in three replicate wells.

Alkaline Phosphatase Staining and Activity

Cells (hASCs and hBMSCs) were seeded in six-well plates. After 7 days of osteoinduction, alkaline phosphatase (ALP) staining

Table 1. Sequences of RNA and DNA oligonucleotides

Name	Sense strand/sense primer (5′-3′)	Antisense strand/antisense primer (5′-3′)
Primers		
PCK2	GAGTGTTTCCCTCCCCAAGG	GCGTGCCTTTGGTGATTCAG
PCK1	CATCCACATCTGTGACGGCTCTG	TCTTTGCTCTTGGGTGACGATAA
RUNX2	CCGCCTCAGTGATTTAGGGC	GGGTCTGTAATCTGACTCTGTCC
OCN	CACTCCTCGCCCTATTGGC	CCCTCCTGCTTGGACACAAAG
GAPDH	GGTCACCAGGGCTGCTTTT	GGATCTCGCTCCTGGAAGATG
ALP	GACCTCCTCGGAAGACACTC	TGAAGGGCTTCTTGTCTGTG
ATG7	AGCGGCGGCAAGAAATAA	CCAGCCGATACTCGTTCA
LC3B	GCACCTTCGAACAAAGAGTAGA	GCACCTTCGAACAAAGAGTAGA
P62	AGAGCAGCAGCGTCAGGAA	ACGCCAAACTGTTGTAGGACTT
ULK1	CCTGCTGAGCCGAGAATG	CTGCTTCACAGTGGACGACA
shRNA		
Control	TTCTCCGAACGTGTCACGT	
sh1-*PCK2*	GGTGGCAAGCATGCGTATTAT	
sh2-*PCK2*	GGGATGATATTGCTTGGATGA	
sh1-ATG7	CAAGGACATTAAGGGTTATTA	
sh2-*ATG7*	TCCAAAGTTCTTGATCAATAT	
si-RNA		
si1-*ULK1*	GGUACCUCCAGAGCAACAUTT	AUGUUGCUCUGGAGGUACCTT
si2-ULK1	GGCUGAAUGAGCUGUACAATT	UUGUACAGCUCAUUCAGCCTT
si-AMPK	CGGGAUCAGUUAGCAACUAdTdT	AGUUGCUAACUGAUCCCGdTdT
Negative control	UUCUCCGAACGUGUCACGUTT	ACGUGACACGUUCGGAGAATT

Abbreviations: shRNA, short-hairpin RNA; si-RNA, short interfering RNA.

and activity were conducted according to previously established protocols [22]. The 5-bromo-4-chloro-3-indolyl-phosphate/Nitro-Blue-Tetrazolium staining kit (CoWin Biosciences, Beijing, China), bicinchoninic acid (BCA) protein assay kit (Prod#23225, Pierce Thermo Scientific, Waltham, MA) and ALP assay kit (A059-2, Nanjing Jiancheng Bioengineering Institute, Nanjing, China) were used.

Alizarin Red S Staining and Quantification

For alizarin red S (ARS) staining and quantification, hASCs were seeded in six-well plates. On the 14th day of osteoinduction, cells were fixed with 95% ethanol for 30 minutes at room temperature. After washed with distilled water for three times, the cells were incubated with ARS solution (2%, pH 4.2, Sigma–Aldrich). For quantification, the plate was incubated with 100 mM cetylpyridinium chloride (Sigma–Aldrich) for 1 hour and the solution was collected. According to previously established protocols [23, 24], the absorbance of solution was measured at 562 nm and normalized to the total protein concentration.

RNA Collection and Quantitative Reverse Transcription Polymerase Chain Reaction

Cells (hASCs and hBMSCs) were seeded in six-well plates, and total cellular RNA was extracted after 7 and 14 days of osteoinduction. Quantitative real-time PCR was conducted as described previously [25]. The expression of glyceraldehyde 3-phosphate dehydrogenase (GAPDH) was detected for normalization of gene expression. The primers used for PCK2, PCK1, GAPDH, ATG7, RUNX2, ALP, OCN, LC3B, p62, and ULK1 are listed in Table 1. To analyze the fold differences in relative expression, the cycle threshold values (Ct values) were calculated using the $2^{-\Delta\Delta Ct}$ method.

Immunofluorescence Staining

The hASCs were seeded on confocal plates cultured in PM and OM, separately. After 7 days, cells were fixed in 4% paraformaldehyde and treated as previously described [26]. The antibody (1:200 dilution) against the autophagy marker LC3B was from Cell Signaling Technology (Danvers, MA) and goat anti-rabbit fluoresceine isothiocyanate (green, 1:150 dilution) was from Gibco. DAPI (blue) was used for staining nuclei. Fluorescence staining was visualized using a Confocal Zeiss Axiovert 650 microscope with the appropriate excitation wavelengths.

Western Blot Analysis

The total protein of hASCs or hBMSCs were prepared in radioimmunoprecipitation assay buffer including protease inhibitor mixture (Roche Applied Science, Mannheim, Germany) and phosphatase inhibitors (Keygenbio China, kgp602). Then the lysates were harvested and centrifuged at 14,000 rpm at 4°C for 15 minutes. The protein concentration was measured by using Pierce BCA protein assay kit (Thermo Scientific). Equal amount of the protein extracts was separated on proper SDS-PAGE (7.5%, 10%, or 15%) and transferred to polyvinylidene difluoride membrane (Bio-Rad). After blocking in 5% milk for

2 hours, the membranes were incubated with the primary antibodies at 4°C overnight. The electrochemiluminescence (ECL) kit (CWBIO) was used to detect the protein bands after incubation with secondary antibodies at room temperature for 1 hour. The following antibodies were used and diluted 1:1,000; Cell Signaling Technology: PCK2 (8565), PCK1 (12940), LC3B (2775), SQSTM1/p62 (88588), RUNX2 (12556), ATG7 (8558), ULK1 (8054), and phospho-AMPK α (2635); Abcam (Cambridge, UK): phospho-ULK1 (Ser 556; ab203207), phospho-ULK1 (Ser 555; ab229537), phosphor-ULK1 (Ser 757; ab6888), and AMPK (Ab32047); Huaxingbochuang Biotechnology (Beijing, China): GAPDH (HX1832).

Heterotypic Bone Formation Assay in Vivo

The hASCs stably infected with NC, sh1-*PCK2*, sh2-*PCK2*, *PCK2*, and vector, *PCK2* + sh1-*ATG7*, *PCK2* + si-*ULK1* were mixed with beta-tricalcium phosphate (β-TCP; Bicon, Boston, MA) particles. The complexes were implanted subcutaneously under the dorsal space of 42-day-old, BALB/c homozygous nude (nu/nu) mice (*n* = 10 mice per group, each experiment was performed three times). The specific procedure for nude mouse implantation has been previously described [22–24]. The Institutional Animal Care and Use Committee of the Peking University Health Science Center approved the performance of this study (LA2014233) and all in vivo experiments were conducted in accordance with Institutional Animal Guidelines.

Micro-Computed Tomography Analysis of Xenograft Mice

To assess the mass and shape of the new bone among each group, the specimens were scanned with an Inveon MM system (Siemens, Munich, Germany) after fixation as previously described [27]. The scanning conditions were an X-ray voltage of 80 kV, current of 500 μA, and exposure time of 1,500 ms for each of the 360 rotational steps. For quantification of the images, BV/total volume (TV) [28] was calculated using an Inveon Research Workplace (Siemens). Image-Pro Plus software (Media Cybernetics, Rockville, MD) was used to measure the percentage of new bone or collagen formation area [(bone or collagen area/total tissue area) * 100%]. Quantitative results were exhibited by histograms.

OAA Concentration Measurement

The hASCs transfected with pcDNA3.1, wild-type, and mutant PCK2 were incubated with 4 μg OAA (Macklin, 328-42-7) for 1 hour and the cells were rapidly homogenized with OAA assay buffer. The remnant OAA concentration was measured according to the protocol of OAA assay kit (Sigma, MAK070). The concentrations of OAA were calculated by building the calibration curve for 0–1 nmole per well standards.

Analyses of Bone Formation In Vivo

Samples were collected after 8 weeks and fixed in 4% paraformaldehyde for 24 hours. Samples were decalcified for 14 days using 10% ethylene diamine tetra acetic acid (EDTA; pH 7.4). Samples were then dehydrated and embedded in paraffin. Next, sections were cut into 5–6 μm thick slices and stained with hematoxylin and eosin (H&E) and Masson's trichome. An inverted fluorescent microscope (Olympus Co., Tokyo, Japan) was used for visualization and analysis of tissue slices.

Statistical Analysis

SPSS Statistics 20.0 software (IBM, Armonk, NY) was used for statistical analysis. The results are presented as a summary of the mean of three independent experiments and data were indicated as mean ± SD. For comparisons between two experimental groups, Student's *t* test was used. A two-tailed *p*-value ≤.05 was considered to indicate statistical significance.

RESULTS

PCK2 Promotes Osteogenic Differentiation of MSCs

To explore PCK2 impact upon MSCs as they differentiate toward osteogenic lineages, stable hASCs and hBMSCs cell lines transfected with lentivirus for *PCK2* knockdown or overexpression were constructed. Two shRNA sequences targeting *PCK2* were used to avoid off-target effects. The lentiviral transduction efficiency of hASCs was confirmed by fluorescent staining (Supporting Information Fig. S1A), quantitative reverse transcription polymerase chain reaction (qRT-PCR; Supporting Information Fig. S1B, S1C), and Western blottings (Fig. 1A; Supporting Information Fig. S1D). Moreover, CCK-8 assays (Supporting Information Fig. S1E, S1F) demonstrated that changes in PCK2 expression have no obvious effects on cell proliferation. After 7 days of osteogenic induction, we found that PCK2 deficiency resulted in significantly decreased ALP activity (Fig. 1B, 1C; Supporting Information Fig. S2A, S2B). We also measured the mRNA expressions of osteogenic markers by qRT-PCR. PCK2 knockdown significantly decreased the expression of *Runt-related transcription factor 2* (*RUNX2*) and *ALP* after 7 days of osteogenic induction (Fig. 1D, 1E; Supporting Information Fig. S2C, S2D). After 14 days of osteogenic differentiation, ARS staining and quantification, indicating extracellular matrix mineralization, was also decreased after depletion of PCK2 (Fig. 1F, 1G; Supporting Information Fig. S2E, S2F). Moreover, the relative mRNA expression of *RUNX2* and *osteocalcin* (*OCN*) were reduced in PCK2 knockdown cells after 14 days of osteogenic induction (Fig. 1H, 1I; Supporting Information Fig. S2G, S2H). In addition, overexpression of PCK2 enhanced ALP activity (Fig. 2A, 2B). Overexpressing PCK2 resulted in an increase in the relative mRNA expression levels of *RUNX2* and *ALP* after 7 days of osteogenic differentiation (Fig. 2C, 2D). In addition, PCK2 overexpressing cells demonstrated more extracellular matrix mineralization (Fig. 2E, 2F) and elevated gene expression of osteogenic markers after 14 days of osteogenic induction (Fig. 2G, 2H). Moreover, compared with control cells, the protein level of RUNX2 was upregulated in PCK2 overexpressing cells (Fig. 2I) and was downregulated in PCK2 deficient cells (Fig. 2L; Supporting Information Fig. S2I).

In confirmation of the PCK2-regulated osteogenic differentiation of hASCs as a general phenomenon, we constructed stable cell lines of hBMSCs transfected lentivirus for PCK2 knockdown and overexpression. The transfection efficiency was confirmed (Supporting Information Fig. S1G–S1I). The observations suggested similar results when hBMSCs were treated under the same conditions (Supporting Information Fig. S2J–S2Q). Furthermore, as a critical enzyme for glucose anabolism, PCK2 catalyzes OAA to PEP. To assess whether PCK2-mediated osteogenic differentiation is associated with enzymatic activity of PCK2, pcDNA3.1, FLAG-tagged wild-type,
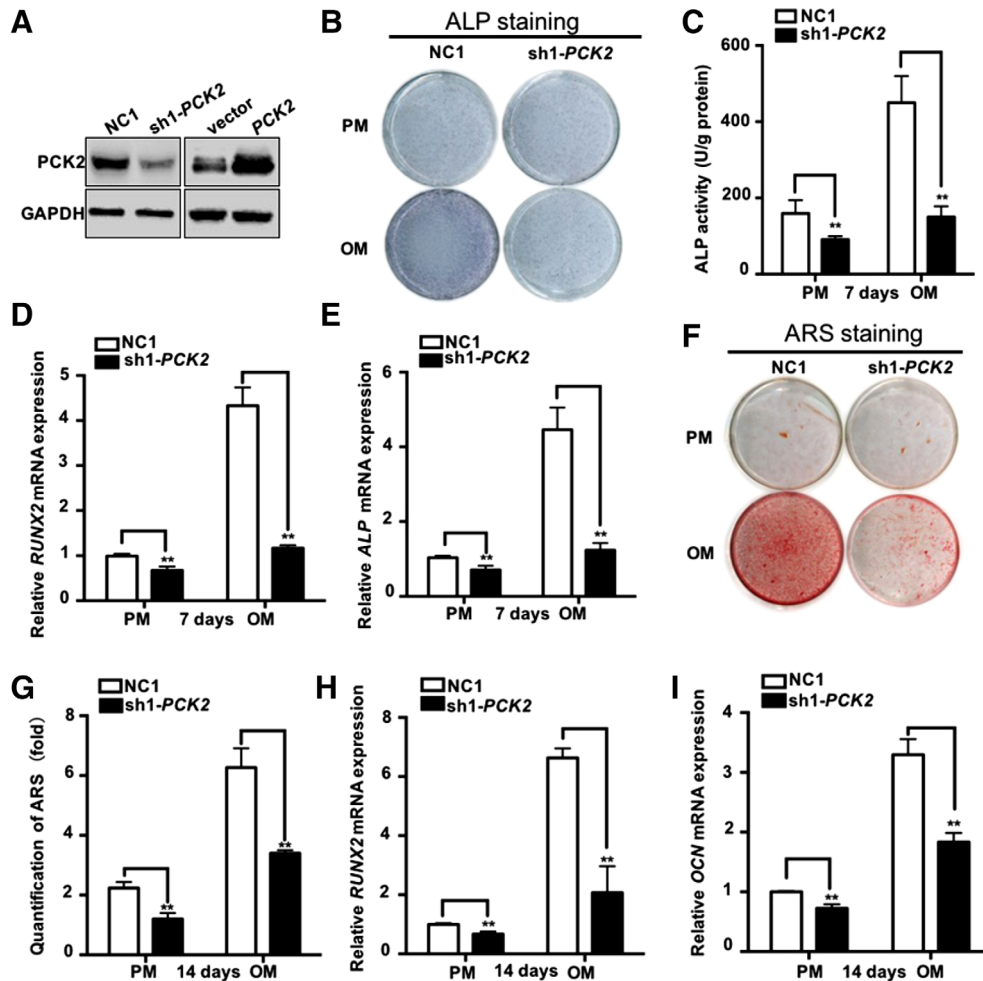
Figure 1. PCK2 knockdown impairs the osteogenic capacity of hASCs in vitro. **(A):** Efficiency of PCK2 knockdown and overexpression was validated by Western blot analysis. GAPDH was used for normalization. **(B, C):** Knockdown of PCK2 decreased ALP staining (B) and activity (C) on the seventh day after osteogenic induction of hASCs. **(D, E):** After 7 days of osteogenic induction, relative mRNA expressions of osteogenic marker *RUNX2* (D) and *ALP* (E) were decreased by the depletion of PCK2. **(F, G):** Extracellular matrix mineralization (F) and ARS quantification (G) were decreased in PCK2 knockdown cells on the 14th day of osteogenic induction. **(H, I):** Relative mRNA expression of *RUNX2* (H) and *OCN* (I) were downregulated by depletion of PCK2 after 14 days of osteogenic induction. Data represent three independent experiments and values are presented as mean ± SD. **, $p \leq .01$; *, $p \leq .05$; Student's t test. Abbreviations: ALP, alkaline phosphatase; ARS, alizarin red S; hASCs, human adipose-derived stem cells; NC1, negative control for sh1-PCK2; OCN, osteocalcin; OM, osteogenic media; PCK2, mitochondrial phosphoenolpyruvate carboxykinase; PM, proliferation media; RUNX2, runt-related transcription factor 2.

and mutant PCK2 plasmids were transfected in hASCs. After incubation of 4 μg OAA for 1 hour, the remnant OAA concentration in hASCs were measured showing that the remnant OAA concentration was relatively higher in mutant PCK2 group than wild-type group (Supporting Information Fig. S2R). The mutant PCK2 transfection decreased ALP activity during osteogenic differentiation, compared with wild-type PCK2 group (Supporting Information Fig. S2S, S2T). Collectively, these data demonstrate that PCK2 is a positive regulator of the osteogenic capacity of MSCs in vitro.

PCK2 Enhances Ectopic Bone Formation from hASCs In Vivo

The in vitro results suggest that PCK2 exerts a vital regulatory effect on osteogenesis by hASCs and we next explored whether PCK2 plays an important role in bone formation in vivo. The hASCs expressing *PCK2*, sh1-*PCK2*, and sh2-*PCK2* were mixed

with β/TCP, separately, and the complexes were implanted into nude mice ($n = 10$ for each group). The samples were harvested at 8 weeks. According to representative images of H&E staining, hASCs/sh1-*PCK2* cells and hASCs/sh2-*PCK2* cells formed much less osteoid tissues, with some scaffold remnants, compared with control cells (Fig. 3A). Simultaneously, lower amounts of organized extracellular matrix with collagen fiber accumulated in PCK2 knockdown groups (blue color as indicated by Masson's trichrome staining; Fig. 3B). Histomorphometry analysis of bone-like tissues illustrated that the area of bone formation was markedly decreased in PCK2 knockdown groups compared with the control group (Fig. 3A, B). Consistently, micro-CT analysis also suggested that PCK2 knockdown groups exhibited less new bone formation and more scaffold remnants (Fig. 3C). Quantifications of micro-CT images further displayed that the percentage of BV to TV in the PCK2 knockdown groups was less than the control group. In contrast, overexpression of PCK2 resulted
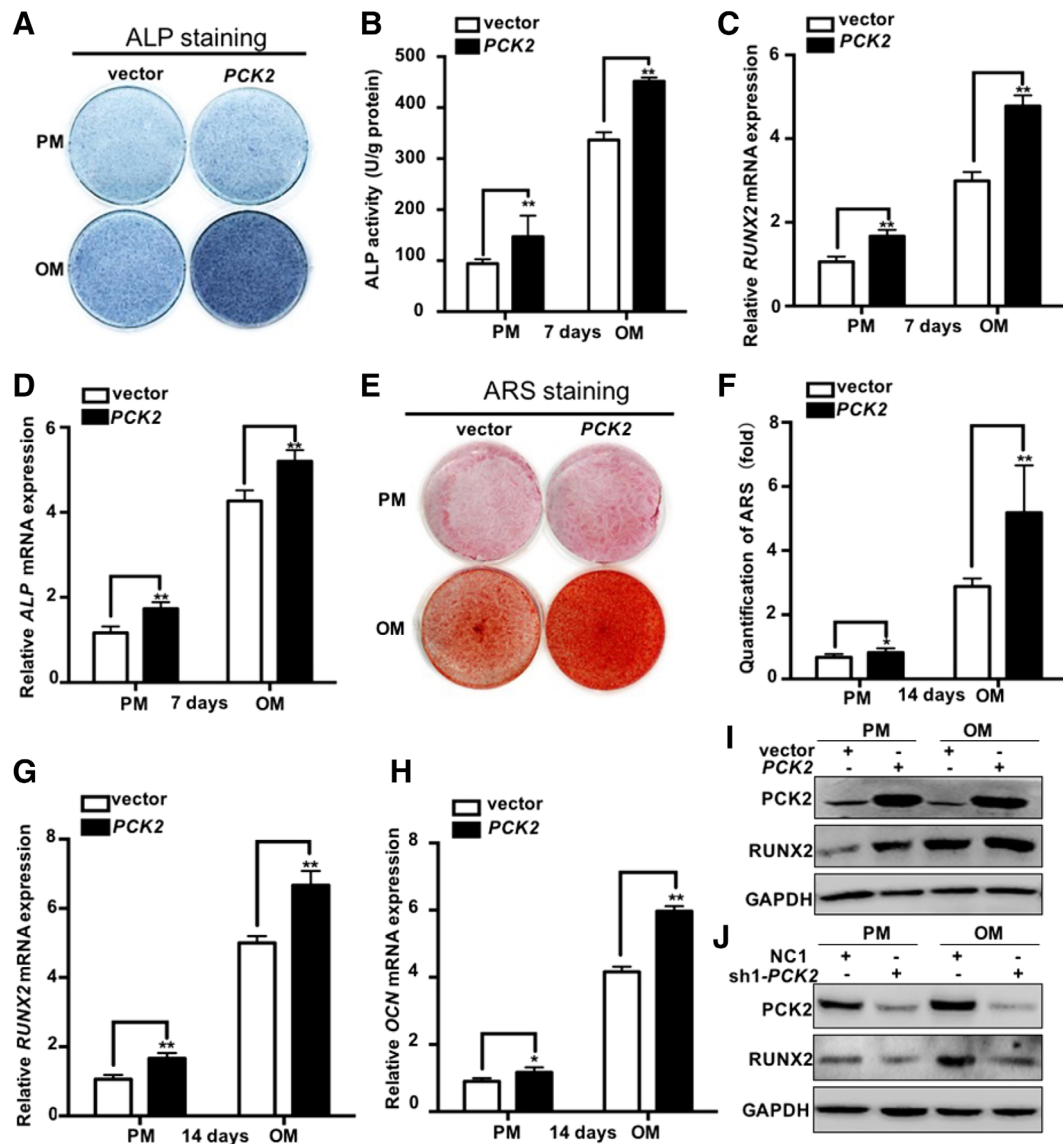
Figure 2. PCK2 overexpression enhances the osteogenic capacity of hASCs in vitro. **(A, B):** Overexpression of PCK2 significantly increased ALP staining (A) and activity (B) after 7 days of osteogenic induction. **(C, D):** PCK2 overexpression upregulates relative mRNA expression of *RUNX2* (C) and *ALP* (D) after 7 days of osteogenic differentiation. **(E, F):** The ARS staining (E) and quantification (F) showed an increasing trend after overexpression of PCK2. **(G, H):** Osteogenic gene markers *RUNX2* (G) and *OCN* (H) were unregulated on the 14th day of osteogenic differentiation. **(I, J):** Knockdown of PCK2 downregulated the protein level of RUNX2 (I) while PCK2 overexpression upregulated RUNX2 expression (J). GAPDH was used for normalization. Data represent three independent experiments and values are presented as mean $\pm$ SD. **, $p \leq .01$; *, $p \leq .05$; Student's *t* test. Abbreviations: ALP, alkaline phosphatase; ARS, alizarin red S; OCN, osteocalcin; OM, osteogenic media; PCK2, mitochondrial phosphoenolpyruvate carboxykinase; PM, proliferation media; RUNX2, runt-related transcription factor 2.

in much more uniform, acidophilic osteoid tissue as shown by H&E staining, compared with the control vector group, including some microvascular formation (Fig. 3D). Meanwhile, more organized extracellular matrix with collagen fiber accumulation (Fig. 3E) was shown in PCK2-expressing group. Consistently, micro-CT and quantitative measurement also demonstrated that the percentage of BV to TV in the PCK2 overexpression group was more than the control group (Fig. 3F). These results displayed similar outcomes to the in vitro findings (Figs. 1 and 2; Supporting Information Figs. S1 and S2) and further confirmed that PCK2 enhances the osteogenic differentiation, thereby promoting ectopic bone formation in vivo (Fig. 3).

PCK2 Modulates Autophagy During Osteogenic Differentiation

Our results indicated that PCK2 plays a significant role in promoting osteogenic differentiation of MSCs, but the regulatory mechanism involved in this process remained unclear. Because autophagy is an important process in protecting stem cells from metabolic stress [29], we next examined whether PCK2 is involved in regulating autophagy of MSCs. Microtubule associated protein 1 light chain 3 β (LC3B) accumulation and p62/SQSTM1 (p62) degradation were used as two biological markers of autophagy [30], and were evaluated by immunoblotting. Treatment with H_2O_2 (500 μM)-induced p62
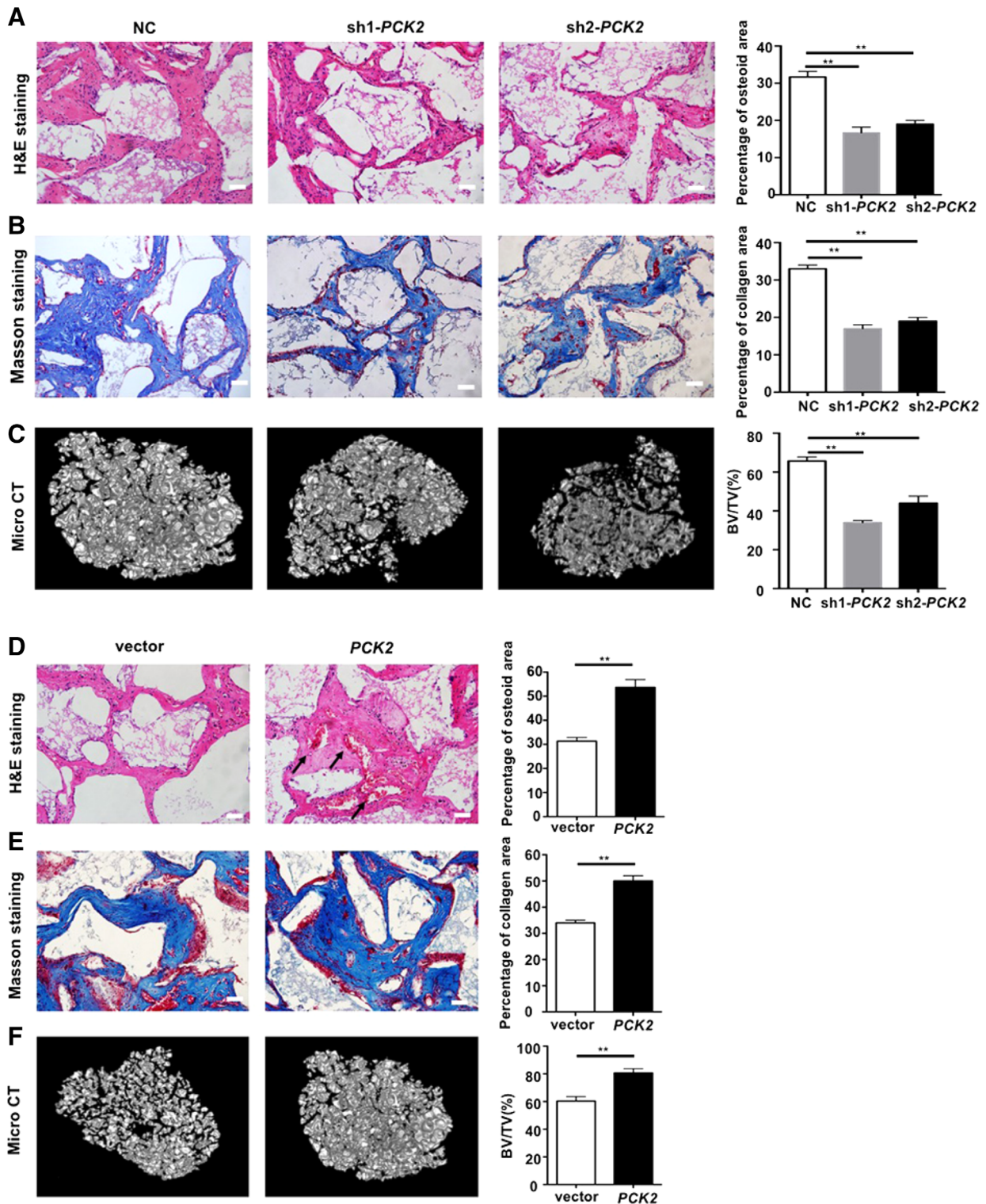
Figure 3. PCK2 enhances hASC osteogenesis in vivo. The hASCs transfected with sh1-*PCK2*, sh2-*PCK2*, NC, *PCK2*, and vector were mixed with β-TCP carriers and were subcutaneously implanted into the dorsal side of the mice. After 8 weeks, the samples were harvested. **(A, B, D, E):** H&E staining (A, D), Masson's trichrome staining (B, E) and the histomorphometry analysis of the implanted hASC-scaffold hybrids are presented. **(C, F):** Representative micro-CT images and quantitative analysis of BV/TV (%) are shown. H&E staining of implanted hASCs-TCP hybrids is presented. The black arrows in (D) point to microvascular formation. Scale bar = 100 μm. Images are representative of three independent experiments, each including 10 BALB/c nude mice. Results are presented as the mean ± SD, n = 3. *, $p < .01$; **, $p < .05$. Abbreviations: BV/TV, bone volume to total volume; hASCs, human adipose-derived stem cells; H&E, hematoxylin and eosin; β-TCP, beta-tricalcium phosphate; NC, negative control for sh1-PCK2 and sh2-PCK2; PCK2, mitochondrial phosphoenolpyruvate carboxykinase.
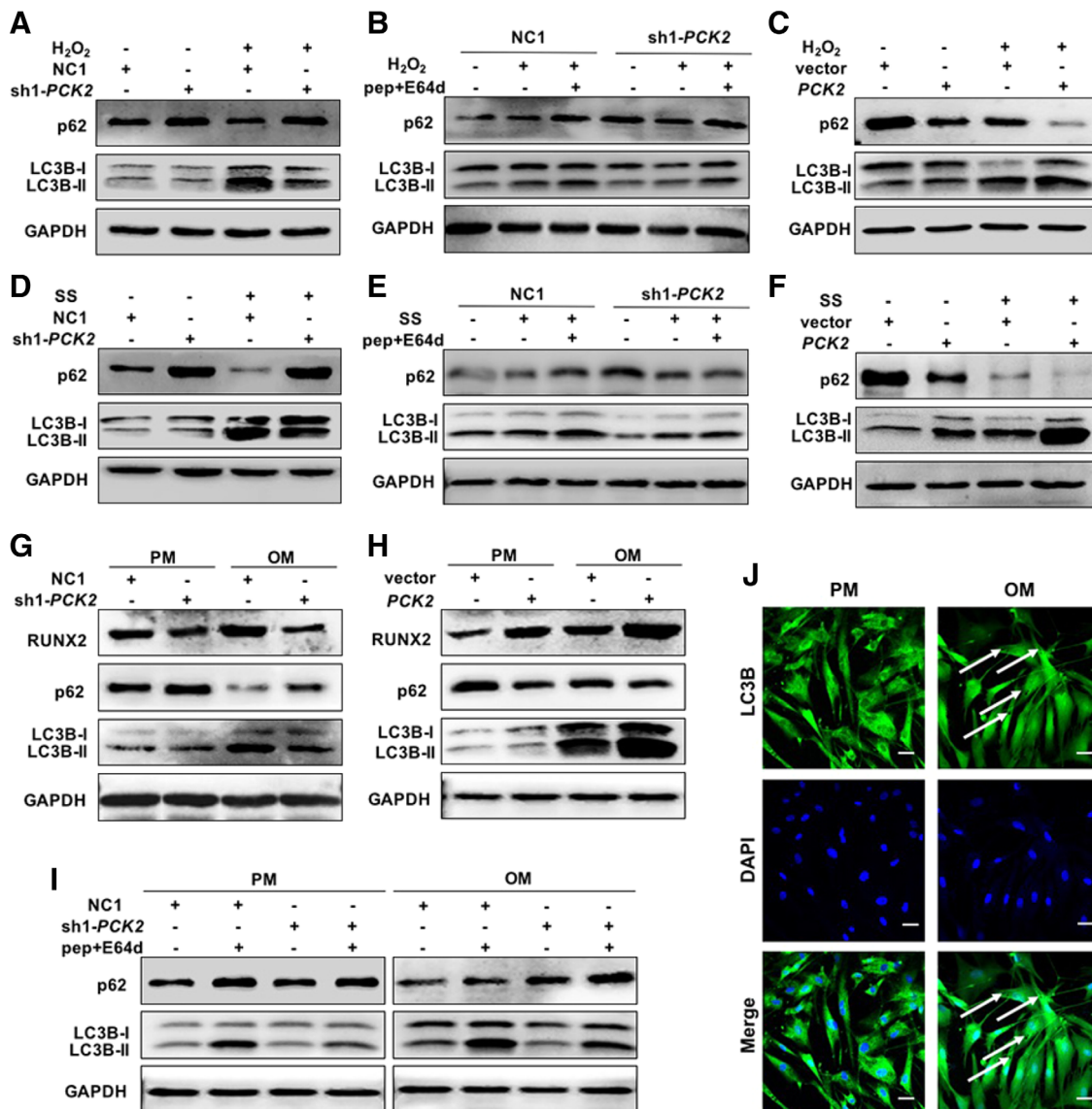
Figure 4. PCK2 positively regulates autophagy during osteogenesis by hASCs. **(A):** PCK2 knockdown and control cells were cultured in regular PM or PM containing 500 μM H_2O_2 for 24 hours. **(B):** The control cells or PCK2 knockdown cells were cultured in PM, PM containing 500 μM H_2O_2, or PM containing 500 μM H_2O_2 and 10 μg/ml pep + E64d for 24 hours. **(C):** The control vector cells or PCK2-expressing and cells were cultured in PM or PM containing 500 μM H_2O_2 for 24 hours. **(D):** The control cells or PCK2 knockdown cells were cultured in PM or PM without serum (SS medium) for 48 hours. **(E):** The sh1-*PCK2* or NC1 cells were cultured in PM, SS medium, or SS medium containing 10 μg/ml pep + E64d for 48 hours. **(F):** The PCK2-expressing and control vector cells were cultured in PM or SS medium for 7 days. **(G, H):** The control cells and PCK2 knockdown cells were cultured in PM or OM (G). The control vector cells and PCK2-expressing cells were cultured in PM or OM (H). **(I):** The control cells and PCK2 knockdown cells were cultured in PM and OM, with or without 10 μg/ml pep + E64d for 7 days. **(J):** Confocal microscopy of LC3B with DAPI counterstaining on the seventh day of osteogenic induction. Scale bars = 100 μm. Images represent three independent experiments. GAPDH was used as loading control. Abbreviations: DAPI, 4′,6-diamidino-2-phenylindole; LC3B, microtubule associated protein 1 light chain 3 β; NC1, negative control for sh1-*PCK2*; OM, osteogenic media; PCK2, mitochondrial phosphoenolpyruvate carboxykinase; p62, p62/SQSTM1; pep: pepstain A; PM, proliferation media; OM, osteogenic media; RUNX2, runt-related transcription factor 2; SS, serum starvation.

degradation or accumulation of LC3B in control cells, but not in PCK2 knockdown cells (Fig. 4A; Supporting Information Fig. S3A). However, the increase in LC3B not only demonstrates increased autophagy flux, but also indicates the inhibition of autophagosome degradation [31]. To measure the autophagy flux precisely, protease inhibitors E64d (10 μg/ml) and pepstatin A (pep, 10 μg/ml) were used to suppress the fusion of autophagosomes with the lysosome, resulting in the accumulation of LC3B and the blockade of p62 degradation. H_2O_2 treatment significantly

increased autophagy flux in control cells, but not in PCK2 knockdown cells (Fig. 4B; Supporting Information Fig. S3F), further suggesting that depletion of PCK2 markedly suppresses autophagy. Meanwhile, compared with the control group, overexpression of PCK2 promoted the accumulation of LC3B and the degradation of p62 (Fig. 4C; Supporting Information Fig. S3D). To confirm the positive regulatory effect of PCK2 on autophagy, we assessed autophagy flux in cells cultured under conditions of serum starvation with or without pep + E64d. As expected, we observed a
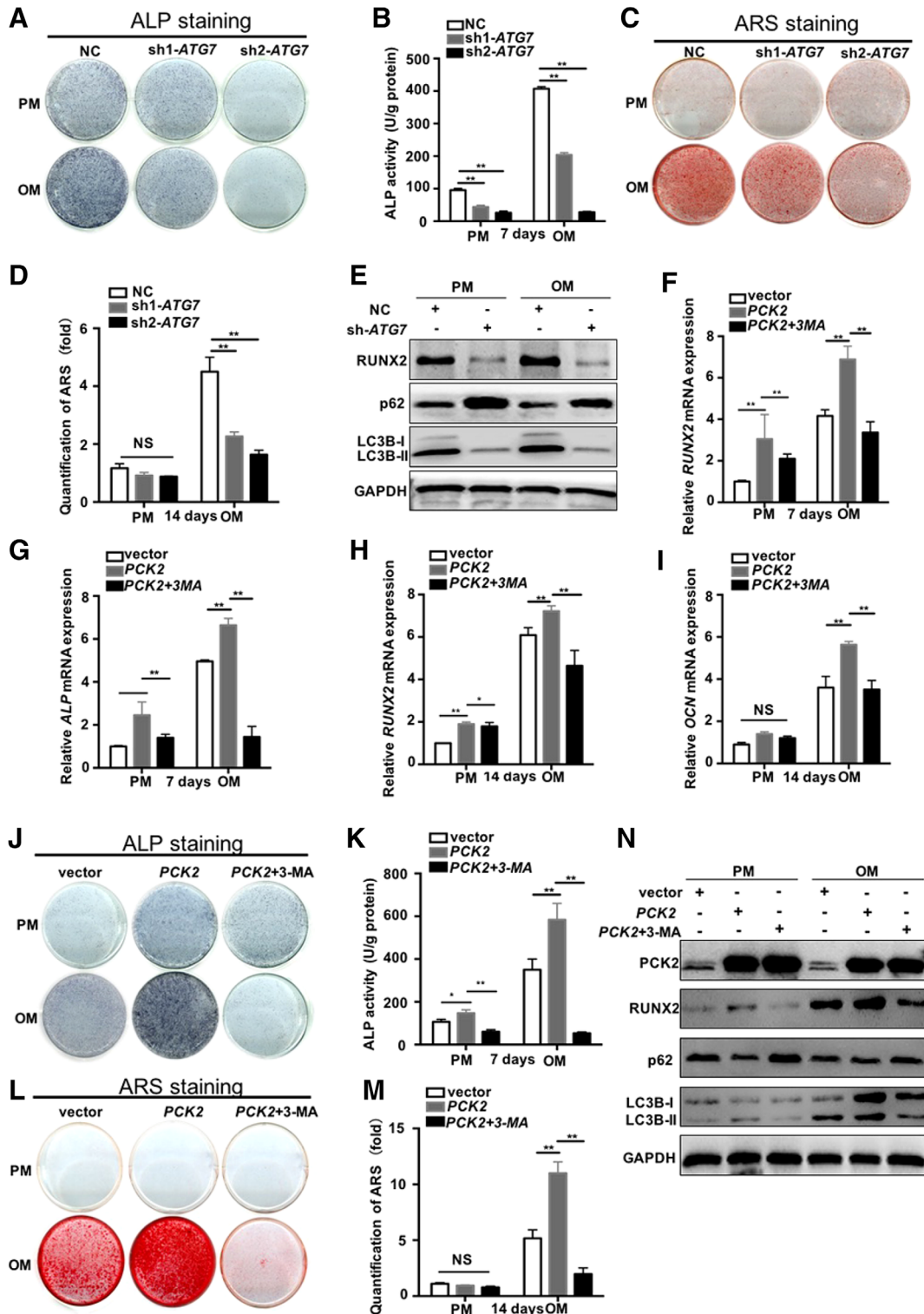
Figure 5. Autophagy is required for the osteogenic differentiation of hASCs. **(A, B):** Depletion of ATG7 decreased ALP staining (A) and activity (B) on the seventh day after induction of osteogenic differentiation of hASCs. **(C, D):** Extracellular matrix mineralization (C) and ARS quantification (D) were decreased in ATG7 knockdown cells after 14 days of osteogenic induction. **(E):** Protein levels of RUNX2, p62, and LC3B are indicated as shown. GAPDH was used as internal loading control. **(F–M):** Treatment with 5 mM 3-MA decreased the osteogenic capacity of PCK2-expressing cells. Relative mRNA expression of *RUNX2* (F) and *ALP* (G) on the seventh day of osteogenic induction are shown. Relative mRNA expression of *RUNX2* (H) and *OCN* (I) after 14 days of osteogenic induction is shown. ALP staining (J) and activity (K) on the seventh day of osteogenic induction are shown. Extracellular matrix mineralization (L) and ARS quantification (M) on the 14th day of osteogenic induction are presented. **(N):** Protein expression patterns of PCK2, RUNX2, p62, and LC3B are shown. The control vector cells and PCK2-expressing cells were cultured in PM, PM containing 5 mM 3-MA, OM, or OM containing 5 mM 3-MA for 5 days.
(Figure legend continues on next page.)

similar trend to the treatment with H_2O_2 (Fig. 4D–4F; Supporting Information Fig. S3B, S3E). Altogether, these results demonstrate that PCK2 plays an important role in enhancing autophagy of MSCs.

To investigate whether PCK2 exerts a regulatory influence on autophagy during osteogenic differentiation, we examined the autophagy flux of hASCs after 7 days of osteogenic induction. The increasing level of RUNX2 protein determined the osteogenic differentiation of hASCs (Fig. 4G and Supporting Information Fig. S3C). In contrast to the control cells, a dramatic decrease of LC3B and reduced p62 degradation were observed in PCK2 knockdown cells cultured in OM. Concurrently, after 7 days of osteogenic induction, overexpression of PCK2 increased autophagy compared with the control vector group, as demonstrated by increased aggregation of LC3B and degradation of p62 (Fig. 4H). These results demonstrate that PCK2 positively regulates autophagy during osteogenesis by MSCs.

To further evaluate the dynamic variation of autophagy flux during osteogenesis by MSCs, LC3B turnover was measured after pep + E64d treatment. During osteogenic differentiation of hASCs, knockdown of PCK2 significantly reduced autophagy flux (Fig. 4I). The similar trend was observed during osteogenic differentiation of hBMSCs (Supporting Information Fig. S3H). In addition, autophagosomes were observed by fluorescence microscopy, indicated by a marked increase in LC3B puncta after osteogenic induction (Fig. 4J). Based on these data, it can be inferred that PCK2 regulates osteogenic differentiation of MSCs through modulating autophagy.

Autophagy Is Indispensable for Osteogenic Differentiation

We investigated the specific role of autophagy as a regulator of osteogenesis by hASCs. ALP activity and ARS staining/quantification were used to confirm the osteogenic capacity of hASCs (Supporting Information Fig. S4A–S4C). Western blot analysis showed that LC3B accumulates during osteogenic differentiation, accompanied by degradation of p62 (Supporting Information Fig. S5A, S5B). Gene expressions determined by qRT-PCR corroborated these findings (Supporting Information Fig. S4D–S4F). These data suggest that autophagy is involved in hASCs osteogenic differentiation.

Autophagy is a multistep process and can be suppressed at different stages [32]. To examine the regulatory effect of autophagy on osteogenic capacity, we used two classic inhibitors of autophagy: 3-methyladenine (3-MA, 5 mM), which suppresses phosphoinositide 3-kinases (PI3Ks), and chloroquine (10 μM), which impairs the fusion of the autophagosome to the lysosome. Both inhibitors blocked osteogenesis by hASCs as demonstrated by a decrease in ALP activity (Supporting Information Fig. S4G–S4J) and reduced expression of *RUNX2* mRNA (Supporting Information Fig. S4K–S4L).

To further substantiate the regulatory effects of autophagy on osteogenesis, two lentiviral sequences encoding sh-*ATG7* and the scrambled control shRNA (NC) were transfected into hASCs. Transduction efficiency was confirmed by immunofluorescence, qRT-PCR (Supporting Information Fig. S5C, S5D), and Western blot (Supporting Information Fig. S5E). After 7 days of osteogenic induction, depletion of ATG7 downregulated ALP activity (Fig. 5A, 5B). Moreover, the extracellular matrix mineralization and quantification were also decreased in ATG7 depleted cells after 14 days of osteogenic induction (Fig. 5C, 5D). Furthermore, qRT-PCR results demonstrated a corresponding reduction in the relative mRNA level of osteogenic-related marker genes at the 7th (Supporting Information Fig. S5F, S5G) and 14th days (Fig. 5H, 5I) of osteogenic differentiation. During the course of osteogenic differentiation, knockdown of ATG7 led to significant impairment of autophagy flux and inhibited osteogenic differentiation of hASCs (Fig. 5E), as indicated by decreased RUNX2 protein expression. Altogether, these data show that activation of autophagy is necessary for the osteogenesis by hASCs.

PCK2 Promotes Osteogenic Differentiation by Regulating AMPK/ULK1-Mediated Autophagy

To precisely assess the regulatory effects of PCK2 on osteogenic differentiation through autophagy, 3-MA, which inhibits autophagy activity, was used to treat PCK2-expressing cells. Compared with PCK2-overexpressing cells, the mRNA expression of osteoblastic markers was attenuated in *PCK2* + 3-MA cells during osteogenic induction (Supporting Information Fig. S5F–S5I). Similarly, treatment of cells with 5 mM 3-MA inhibited ALP activity (Fig. 5J, 5K) and reduced ARS staining/quantification (Fig. 5L, 5M), which were enhanced by PCK2 overexpression. Most importantly, upon 3-MA treatment, overexpression of PCK2 failed to elevate osteogenesis in hASCs, as shown by the significant reduction of RUNX2 protein (Fig. 5N). These results prove that PCK2 facilitates osteogenic differentiation of hASCs by regulating autophagy.

As a key initiator of lysosomal-dependent autophagy, unc-51 like autophagy activating kinase 1 (ULK1) serves important roles in cellular nutrient degradation during processes such as glucose metabolism and lipid metabolism [26, 33]. To further explore the molecular mechanism by which PCK2 regulates autophagy during osteogenic differentiation, we performed Western blot analysis to score changes of ULK activity in PCK2 knockdown cells. We found a dramatic increase in ULK1 phosphorylation during osteogenic differentiation, particularly at serine 555 (Ser 555), serine 556 (Ser 556), and serine 757 (Ser 757; Fig. 6A; Supporting Information Fig. S6A). However, knockdown of PCK2 significantly attenuated phosphorylation of ULK1 (Fig. 6A; Supporting Information Fig. S6A). Meanwhile, overexpression of PCK2 led to upregulation of ULK1 phosphorylation at Ser 555, Ser 556, and Ser 757 during osteogenesis (Fig. 6B). AMPK integrates various metabolic signals and can activate ULK1 through phosphorylation at multiple sites [34–36]. Our results indicate that the pattern of AMPK phosphorylation corresponds with ULK1 expression after knockdown or overexpression of PCK2 (Fig. 6A, 6B; Supporting Information Fig. S6A).
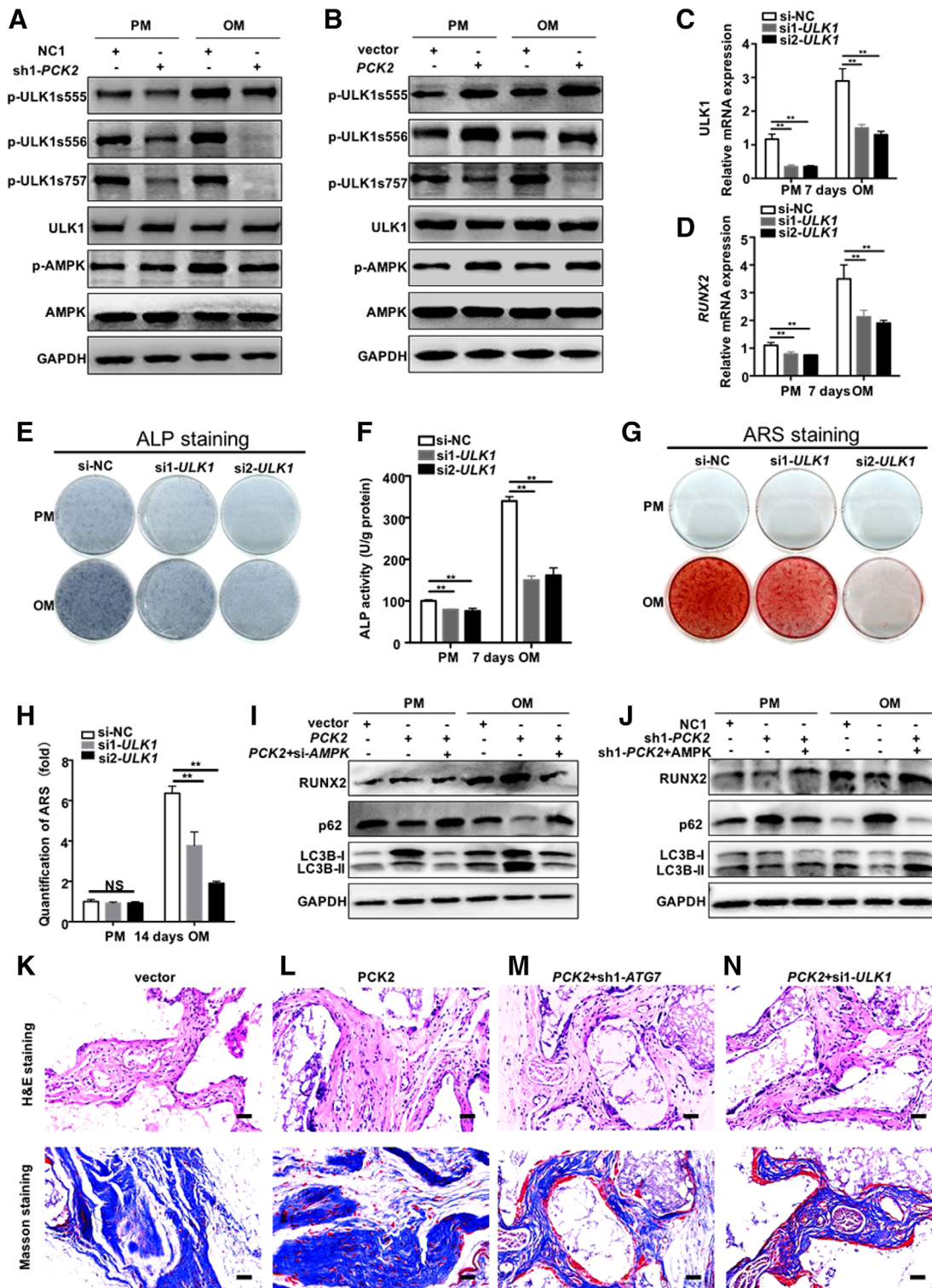

Figure 6. PCK2 enhances osteogenic differentiation of hASCs via modulating AMPK/ULK1-dependent autophagy. **(A):** Protein expression levels of p-ULK1 (ser 555), p-ULK1 (ser 556), p-ULK1 (ser 757), ULK1, p-AMPK α, and AMPK in PCK2-knockdown and control cells are shown. **(B):** Western blots of p-ULK1 (ser 555), p-ULK1 (ser 556), p-ULK1 (ser 757), ULK1, p-AMPK α, and AMPK in PCK2-expressing and control vector cells. **(C, D):** Relative mRNA expression levels of ULK1 (C) and RUNX2 (D) in hASCs transfected with si1-*ULK1*, si2-*ULK1*, and negative control (si-NC) after 7 days of osteogenic induction. Data represent three independent experiments. **(E, F):** Depletion of ULK1 decreases ALP staining (E) and activity (F) on the seventh day after induction of osteogenic differentiation in hASCs. **(G, H):** Knockdown of ULK1 decreases ARS staining (G) and activity (H) on the 14th day after induction of osteogenic differentiation in hASCs. **(I):** Inhibition of AMPK in PCK2-expressing hASCs suppresses osteogenic ability and autophagy activity of hASCs, as shown by the protein expressions of RUNX2, LC3B, and p62. **(J):** PCK2-knockdown cells expressing wild-type AMPK increase the osteogenic capacity and autophagy activity of

(Figure legend continues on next page.)

To examine the potential role of ULK1 during the osteogenesis by hASCs, two si-RNA sequences were used to suppress ULK1 expression, and the knockdown efficiency was confirmed by the qRT-PCR (Fig. 6C). Analysis of the mRNA expression of *RUNX2* (Fig. 6D), ALP activity (Fig. 6E, 6F), and ARS staining/quantification (Fig. 6G, 6H) showed that depletion of ULK1 significantly inhibits osteogenic differentiation of hASCs. These data demonstrate that ULK1 is a positive regulator of osteogenic differentiation. To further explore the regulatory effect of PCK2 on autophagy and osteogenic differentiation through AMPK/ULK1 signaling pathway, si-AMPK was added in the PCK2-expressing cells and wild-type-AMPK plasmid was transfected in the PCK2-knockdown cells. The transfection efficiency was confirmed by Western blot (Supporting Information Fig. S6B). The results displayed that elevated osteogenic capacity and autophagy activity of PCK2-overexpression cells was significantly suppressed by the inhibition of AMPK (Fig. 6I), whereas the decreased osteogenic ability and autophagy activity induced by PCK2 inhibition was rescued by overexpression of AMPK (Fig. 6J). To verify our in vitro findings, we next investigated the potential role of AMPK/ULK1 on osteogenic differentiation in vivo. H&E staining, Masson's trichrome staining from implanted hASC-scaffold hybrids demonstrated that inhibiting ATG7 or suppressing ULK1 expression in PCK2-expressing cells led to significant suppression of osteogenic differentiation (Fig. 6K–6N). Altogether, these findings suggest that PCK2 regulates osteogenic differentiation through AMPK/ULK1-mediated autophagy.

DISCUSSION

The important effects that PCK2 exerts in regulating gluconeogenesis and the TCA cycle ideally fulfill the energy requirements of MSCs osteogenic differentiation, and prompted us to examine the roles of PCK2 in the osteogenic capacity of MSCs. The increasing energy demands on MSCs during osteogenic differentiation not only require increased anabolism, but also require a strict regulation of protein turnover and lysosome-mediated degradation of cellular substances [37]. Autophagy is a catabolic process that efficiently degrades damaged organelles and macromolecules in the lysosome, allowing the nutrients to be recycled under conditions where there the external energy supply is limited [38]. In our current study, we discovered that PCK2 acts as a potent regulator promoting the osteogenic capacity of MSCs, and we unveiled a previously unreported function of PCK2. Our findings extend the knowledge about the molecular mechanisms of PCK2 as a positive factor in the osteogenic differentiation of MSCs. Interestingly, through exploring potential mechanisms, we observed a positive regulatory effect of PCK2 on autophagy during osteogenesis by MSCs. A recent study demonstrated that depletion of autophagy-related-genes, such as *ATG5* and *BECN*, leads to impaired osteogenic ability

of BMSCs in vivo [9]. In accordance with this study, we found that autophagy was indispensable for the osteogenesis by MSCs. More importantly, we demonstrated that PCK2 enhances the osteogenic differentiation through AMPK/ULK1-dependent autophagy. Taken together, our study identified PCK2 as a critical modulator that regulates autophagy and the osteogenic differentiation, demonstrating that PCK2 may be a potential therapeutic target for metabolic bone diseases.

PCK2 is responsible for approximately 50% of the total hepatic PEPCK functions in many mammals, including humans [39–41]. However, the specific biological roles of PCK2 are largely unknown. PCK2 has been reported to be critically involved in modulating glucose metabolism and lipid metabolism [41]. In addition, PCK2 regulates both insulin secretion and gluconeogenesis in order to ensure continuous cataplerotic PEP production [18]. The activity and expression of PCK2 were elevated under low-glucose conditions [42]. In general, PCK2 can be regarded as a key factor in energy metabolism by regulating glucose homeostasis and TCA cycle activity. We speculated that the metaphorical "metabolic tachometer" mechanism enables PCK2 to sense and coordinate appropriate responses to energy changes during the osteogenesis of MSCs. In order to explore the potential role of PCK2, we constructed stable PCK2 knockdown and overexpressing cells and determined the effects of modulating PCK2 expression on the osteogenic capacity of MSCs. Moreover, we observed that PCK2 is involved in positively regulating autophagy. PCK2-deficient cells demonstrated decreased autophagy flux whereas PCK2-overexpressing cells displayed significantly increased autophagy flux. The relationship between PCK2 and autophagy during osteogenesis by hASCs was further examined, and we found that depletion of PCK2 repressed autophagy, resulting in the impairment of the osteogenic ability of MSCs. On the contrary, when PCK2 was overexpressed, we found that autophagy was increased, accompanied by upregulation of osteogenic differentiation of MSCs. Incubation of autophagy inhibitors 3-MA significantly suppressed the osteogenic differentiation of PCK2-overexpression cells. Consistently, inhibition of *ATG7* resulted in the decrease of osteogenic ability in PCK2-expressing cells in vivo, which verifies the idea that PCK2 regulates osteogenic ability of hASCs via modulating autophagy. Therefore, we provide the first demonstration that PCK2 exhibits a positive regulatory effect on osteogenic capacity of MSCs via modulating autophagy. In addition, our results offer a clue that PCK2, which is a critical enzyme for energy metabolism may constitute a new target for innovative therapeutic research in bone pathologies.

Emerging evidence has shown that autophagy is actively involved in the maintenance of bone homeostasis and regulation of skeletal metabolism [29, 43]. However, previous studies have mainly concentrated on terminally differentiated cells in the bone system, such as osteoblasts, osteocytes, and osteoclasts [44, 45], and the potential regulatory role of autophagy in MSCs remains unclear [46]. It was reported that constitutive

(Figure legend continued from previous page.)
hASCs. The protein expression patterns of RUNX2, LC3B, and p62 are presented. GAPDH was used as internal loading control in (A, B) and (I, J). **(K–N):** H&E staining, Masson's trichrome staining from implanted hASC-scaffold hybrids. Scale bar = 100 μm, *n* = 10. Data in this figure represent three independent experiments and are presented as mean ± SD. **, $p \leq .01$; *, $p \leq .05$; Student's *t* test. Abbreviations: ALP, alkaline phosphatase; AMPK, AMP-activated protein kinase; ARS, alizarin red S; ATG7, autophagy-related-gene-7; hASCs, human adipose-derived stem cells; H&E, hematoxylin and eosin; LC3B, Microtubule associated protein 1 light chain 3 β; NS, not significant; OM, osteogenic media; p62, p62/SQSTM1; PCK2, mitochondrial phosphoenolpyruvate carboxykinase; PM, proliferation media; RUNX2, runt-related transcription factor 2; ULK1, unc-51 like autophagy activating kinase 1.

autophagy activity in human bone marrow-derived stem cells (hBMSCs) is upregulated in early stages of osteogenic induction [47]. The activation of autophagy promotes the osteogenic ability of hBMSCs from osteoporotic vertebrae [22]. Moreover, a recent study showed that diminished lineage differentiation could be partly rescued by activation of autophagy in osteoporotic BMSCs [9]. Investigations on the involvement of autophagy in hASCs have displayed similar results. A study reported that the suppression of autophagy led to the activation of the NF-E2-related factor 2 (Nrf2) pathway and the impairment of osteogenic ability of ASCs following stimulation with reactive oxygen species [21]. Consistent with this report, our study showed that the addition of the autophagy inhibitors 3-MA and CQ significantly suppressed the osteogenic capacity of hASCs (Supporting Information Fig. S4G–S4L). We further confirmed the regulatory effects of autophagy on osteogenic differentiation of hASCs by depletion of ATG7. Knockdown of ATG7 inhibited bone formation, as demonstrated by mRNA (Supporting Information Fig. S5F-S5I) and protein (Fig. 5E) expression analysis of bone formation factors. Our results demonstrate that autophagy plays a positive role during the osteogenesis by hASCs.

A close interaction between autophagy and glucose metabolism has long been a focus of study, and the existence of a dynamic feedback between cellular energy balance and autophagy has been established [48, 49]. It has been reported that ULK1 acts as a dual integrator of energy metabolism and autophagy, by sustaining glucose metabolic fluxes through activation of autophagy, especially in conditions of nutritional-shortage [50]. AMPK is another important intracellular energy sensor, and activates autophagy by directly phosphorylating ULK1 [34]. Our data showed that both the phosphorylation of AMPK α subunit and phosphorylation ULK1 were regulated by PCK2 during osteogenic differentiation. In addition, inhibition of AMPK suppressed the osteogenic ability of PCK2-expressing cells, whereas transfection of wild-type AMPK rescued the decreased osteogenic capacity of PCK2-knockdown cells. Furthermore, suppressing of ULK1 expression impaired the osteogenic differentiation of PCK2-expressing cells in vivo. These results suggest that AMPK/ULK1-mediated autophagy is involved in the PCK2-regulated osteogenic differentiation. However, there are still some questions that remain to be explored. For example, while our study elucidated the regulatory function of PCK2 on autophagy and osteogenic differentiation of MSCs, the functional domain of PCK2 involved in this regulation remains unknown. In future studies, we aim to further evaluate the sites on the PCK2 protein, which are directly responsible for its regulatory functions.

CONCLUSION

In conclusion, our current study demonstrates a novel role of PCK2 in promoting bone formation of MSCs. Besides unraveling the function of PCK2 in osteogenic differentiation, our observations also contribute to the understanding of molecular mechanisms governing osteogenic capacity of MSCs. Mechanistically, PCK2 regulates osteogenic differentiation through regulating AMPK/ULK1-dependent autophagy. This newly discovered function for PCK2 could be exploited as a novel metabolic target for maintaining energy homeostasis and could facilitate the development of MSC-based clinical applications to treat bone metabolic diseases.

AUTHOR CONTRIBUTIONS

P.Z., Y. Zhou: conception and design, financial support, data analysis, manuscript editing and final approval of manuscript, revised the manuscript for intellectual content; Z.L.: laboratory work, data collection and analysis, manuscript writing and final approval of manuscript, revised the manuscript for intellectual content; Xuenan Liu, Y.D., Y. Zhu, Xuejiao Liu, L.L., X.Z., Y.L.: laboratory work, data collection and final approval of manuscript, revised the manuscript for intellectual content.

DISCLOSURE OF POTENTIAL CONFLICTS OF INTEREST

The authors indicated no potential conflicts of interest.

DATA AVAILABILITY STATEMENT

The data that support the findings of this study are available from the corresponding author upon reasonable request.

REFERENCES

1 Mihaila SM, Gaharwar AK, Reis RL et al. The osteogenic differentiation of SSEA-4 sub-population of human adipose derived stem cells using silicate nanoplatelets. Biomaterials 2014;35:9087–9099.

2 Huang T, Liu R, Fu X et al. Aging reduces an ERRalpha-directed mitochondrial glutaminase expression suppressing glutamine anaplerosis and osteogenic differentiation of mesenchymal stem cells. STEM CELLS 2017;35:411–424.

3 Guan M, Wei Y, Liu R et al. Directing mesenchymal stem cells to bone to augment bone formation and increase bone mass. Nat Med 2012;18:456.

4 Sato K, Tsuchihara K, Fujii S et al. Autophagy is activated in colorectal cancer cells and contributes to the tolerance to nutrient deprivation. Cancer Res 2007;67:9677–9684.

5 Levine B, Klionsky DJ. Development by self-digestion: Molecular mechanisms and biological functions of autophagy. Dev Cell 2004;6:463–477.

6 Pantovic A, Krstic A, Janjetovic K et al. Coordinated time-dependent modulation of AMPK/Akt/mTOR signaling and autophagy controls osteogenic differentiation of human mesenchymal stem cells. Bone 2013;52:524–531.

7 Nuschke A, Rodrigues M, Stolz DB et al. Human mesenchymal stem cells/multipotent stromal cells consume accumulated autophagosomes early in differentiation. Stem Cell Res Ther 2014;5:140.

8 Zhou Z, Shi G, Zheng X et al. Autophagy activation facilitates mechanical stimulation-promoted osteoblast differentiation and

ameliorates hindlimb unloading-induced bone loss. Biochem Biophys Res Commun 2018;498:667–673.

9 Qi M, Zhang L, Ma Y et al. Autophagy maintains the function of bone marrow mesenchymal stem cells to prevent estrogen deficiency-induced osteoporosis. Theranostics 2017;7:4498–4516.

10 Rui L. Energy metabolism in the liver. Compr Physiol 2014;4:177–197.

11 Mendez-Lucas A, Duarte JA, Sunny NE et al. PEPCK-M expression in mouse liver potentiates, not replaces, PEPCK-C mediated gluconeogenesis. J Hepatol 2013;59:105–113.

12 Montal ED, Dewi R, Bhalla K et al. PEPCK coordinates the regulation of central carbon metabolism to promote cancer cell growth. Mol Cell 2015;60:571–583.

13 Burgess SC, Hausler N, Merritt M et al. Impaired tricarboxylic acid cycle activity in mouse livers lacking cytosolic phosphoenolpyruvate carboxykinase. J Biol Chem 2004;279:48941–48949.

14 Jiang W, Wang S, Xiao M et al. Acetylation regulates gluconeogenesis by promoting PEPCK1 degradation via recruiting the UBR5 ubiquitin ligase. Mol Cell 2011;43:33–44.

15 Latorre-Muro P, Baeza J, Armstrong EA et al. Dynamic acetylation of phosphoenolpyruvate carboxykinase toggles enzyme activity between gluconeogenic and anaplerotic reactions. Mol Cell 2018;71:718.e719–732.e719.

16 Stark R, Pasquel F, Turcu A et al. Phosphoenolpyruvate cycling via mitochondrial phosphoenolpyruvate carboxykinase links anaplerosis and mitochondrial GTP with insulin secretion. J Biol Chem 2009;284:26578–26590.

17 Vincent EE, Sergushichev A, Griss T et al. Mitochondrial phosphoenolpyruvate carboxykinase regulates metabolic adaptation and enables glucose-independent tumor growth. Mol Cell 2015;60:195–207.

18 Stark R, Guebre-Egziabher F, Zhao X et al. A role for mitochondrial phosphoenolpyruvate carboxykinase (PEPCK-M) in the regulation of hepatic gluconeogenesis. J Biol Chem 2014;289:7257–7263.

19 Haeusler RA, Camastra S, Astiarraga B et al. Decreased expression of hepatic glucokinase in type 2 diabetes. Mol Metab 2015;4:222–226.

20 Yokoyama N, Ishimura T, Oda T et al. Association of the PCK2 gene polymorphism with new-onset glucose intolerance in japanese kidney transplant recipients. Transplant Proc 2018;50:1045–1049.

21 Tao J, Wang H, Zhai Y et al. Downregulation of Nrf2 promotes autophagy-dependent osteoblastic differentiation of adipose-derived mesenchymal stem cells. Exp Cell Res 2016;349:221–229.

22 Wan Y, Zhuo N, Li Y et al. Autophagy promotes osteogenic differentiation of human bone marrow mesenchymal stem cell derived

from osteoporotic vertebrae. Biochem Biophys Res Commun 2017;488:46–52.

23 Ge W, Shi L, Zhou Y et al. Inhibition of osteogenic differentiation of human adipose-derived stromal cells by retinoblastoma binding protein 2 repression of RUNX2-activated transcription. STEM CELLS 2011;29:1112–1125.

24 Ge W, Liu Y, Chen T et al. The epigenetic promotion of osteogenic differentiation of human adipose-derived stem cells by the genetic and chemical blockade of histone demethylase LSD1. Biomaterials 2014;35:6015–6025.

25 Jia LF, Wei SB, Gan YH et al. Expression, regulation and roles of miR-26a and MEG3 in tongue squamous cell carcinoma. Int J Cancer 2014;135:2282–2293.

26 Si C, Zheng Y, Shan Z et al. Promotion effects of miR-375 on the osteogenic differentiation of human adipose-derived mesenchymal stem cells. Stem Cell Rep 2017;8:773–786.

27 Tang Y, Lv L, Li W et al. Protein deubiquitinase USP7 is required for osteogenic differentiation of human adipose-derived stem cells. Stem Cell Res Ther 2017;8:186.

28 Liu H, Li W, Liu Y et al. Co-administration of aspirin and allogeneic adipose-derived stromal cells attenuates bone loss in ovariectomized rats through the anti-inflammatory and chemotactic abilities of aspirin. Stem Cell Res Ther 2015;6:200.

29 Hocking LJ, Whitehouse C, Helfrich MH. Autophagy: A new player in skeletal maintenance? J Bone Miner Res 2012;27:1439–1447.

30 Komatsu M, Waguri S, Koike M et al. Homeostatic levels of p62 control cytoplasmic inclusion body formation in autophagy-deficient mice. Cell 2007;131:1149–1163.

31 Mizushima N, Yoshimori T, Levine B. Methods in mammalian autophagy research. Cell 2010;140:313–326.

32 Klionsky DJ, Abdelmohsen K, Abe A et al. Guidelines for the use and interpretation of assays for monitoring autophagy (3rd edition). Autophagy 2016;12:1–222.

33 Shang L, Chen S, Du F et al. Nutrient starvation elicits an acute autophagic response mediated by Ulk1 dephosphorylation and its subsequent dissociation from AMPK. Proc Natl Acad Sci USA 2011;108:4788–4793.

34 Egan DF, Shackelford DB, Mihaylova MM et al. Phosphorylation of ULK1 (hATG1) by AMP-activated protein kinase connects energy sensing to mitophagy. Science 2011;331:456–461.

35 Laker RC, Drake JC, Wilson RJ et al. Ampk phosphorylation of Ulk1 is required for targeting of mitochondria to lysosomes in exercise-induced mitophagy. Nat Commun 2017;8:548.

36 Hoffman NJ, Parker BL, Chaudhuri R et al. Global phosphoproteomic analysis of human skeletal muscle reveals a network of exercise-regulated kinases and AMPK substrates. Cell Metab 2015;22:922–935.

37 Pi H, Li M, Zou L et al. AKT inhibition-mediated dephosphorylation of TFE3 promotes overactive autophagy independent of MTORC1 in cadmium-exposed bone mesenchymal stem cells. Autophagy 2018;16:1–18.

38 Ho TT, Warr MR, Adelman ER et al. Autophagy maintains the metabolism and function of young and old stem cells. Nature 2017;543:205–210.

39 Luo S, Li Y, Ma R et al. Downregulation of PCK2 remodels tricarboxylic acid cycle in tumor-repopulating cells of melanoma. Oncogene 2017;36:3609–3617.

40 Leithner K, Triebl A, Trotzmuller M et al. The glycerol backbone of phospholipids derives from noncarbohydrate precursors in starved lung cancer cells. Proc Natl Acad Sci USA 2018;115:6225–6230.

41 Stark R, Kibbey RG. The mitochondrial isoform of phosphoenolpyruvate carboxykinase (PEPCK-M) and glucose homeostasis: Has it been overlooked? Biochim Biophys Acta 1840;2014:1313–1330.

42 Leithner K, Hrzenjak A, Trotzmuller M et al. PCK2 activation mediates an adaptive response to glucose depletion in lung cancer. Oncogene 2015;34:1044–1050.

43 Rubinsztein DC, Codogno P, Levine B. Autophagy modulation as a potential therapeutic target for diverse diseases. Nat Rev Drug Discov 2012;11:709–730.

44 Nollet M, Santucci-Darmanin S, Breuil V et al. Autophagy in osteoblasts is involved in mineralization and bone homeostasis. Autophagy 2014;10:1965–1977.

45 Liu F, Fang F, Yuan H et al. Suppression of autophagy by FIP200 deletion leads to osteopenia in mice through the inhibition of osteoblast terminal differentiation. J Bone Miner Res 2013;28:2414–2430.

46 Chen X, He Y, Lu F. Autophagy in stem cell biology: A perspective on stem cell self-renewal and differentiation. Stem Cells Int 2018;2018:9131397.

47 Oliver L, Hue E, Priault M et al. Basal autophagy decreased during the differentiation of human adult mesenchymal stem cells. Stem Cells Dev 2012;21:2779–2788.

48 Okamoto S, Asgar NF, Yokota S et al. Role of the alpha2 subunit of AMP-activated protein kinase and its nuclear localization in mitochondria and energy metabolism-related gene expressions in C2C12 cells. Metabolism 2018;90:52–68.

49 Li Y, Jiang J, Liu W et al. microRNA-378 promotes autophagy and inhibits apoptosis in skeletal muscle. Proc Natl Acad Sci USA 2018;115:E10849–E10858.

50 Alizadeh E, Eslaminejad MB, Akbarzadeh A et al. Upregulation of MiR-122 via trichostatin A treatments in hepatocyte-like cells derived from mesenchymal stem cells. Chem Biol Drug Des 2016;87:296–305.

See www.StemCells.com for supporting information available online.